Adaptive Mobile Sensor Positioning for Multi-Static Target Tracking

Pengcheng Zhan, David W. Casbeer, and A. Lee Swindlehurst

Abstract

Unmanned Air Vehicles (UAVs) are playing an increasingly prominent role in both military and civilian applications. In this paper, we focus on the use of multiple UAV agents in a target tracking application where performance is improved by exploiting each agent's maneuverability. Local time-delay and Doppler measurements made at each UAV are used as inputs to an Extended Kalman Filter (EKF) which tracks the target's position and velocity. Two simple metrics are defined to quantify the accuracy of the tracking algorithm, and heading feedback to the UAVs is used to minimize the metric and improve tracking performance. A simplified version of one of the algorithms that reduces computational complexity is also presented. Simulations demonstrate the significant improvement that results when the UAV sensors are allowed to be optimally positioned during tracking.

I. Introduction

Recent improvements in battery, micro-controller, and sensor technologies have resulted in the development of autonomous vehicles that are inexpensive, dependable, and simple to operate. Unmanned Air Vehicles (UAVs) have well-known defense applications and are useful in many civilian applications as well, such as border and coast patrol, fire perimeter monitoring, search and rescue, *etc*. UAVs are particularly well-suited for situations that are too dangerous for direct human monitoring. While a single autonomous UAV can provide information that is otherwise unattainable, cooperation among a team of UAVs can dramatically improve sensing performance [1]–[5]. The mobility of each UAV within the team can be exploited to adaptively reconfigure the sensing array in response to the environment and the actions of the object being sensed [6]–[8]. It is this additional degree of freedom we wish to exploit in a multi-static radar tracking scenario.

Using mobile and controllable sensing platforms is a relatively new area of research, but has attracted considerable attention in the generic sensor network literature. This type of problem is sometimes referred to as *sensor management*. The majority of work in sensor management for target tracking assumes one of four practical observation

This work was supported by the National Science Foundation under Information Technology Research Grant CCF-0428004.

P. Zhan is with ArrayComm LLC, San Jose, CA ezhan@arraycomm.com

D. Casbeer is a PhD student with the Dept. of Electrical and Computer Engineering, Brigham Young University, Provo, UT casbeer@byu.edu

A.L. Swindlehurst is with the faculty of the Dept. of Electrical Engineering and Computer Science, University of California, Irvine swindle@uci.edu

models: range only [9], [10], bearing only [11], [12], range/bearing [2], [13] and more recently, range/range-rate/bearing [14]. These observation models are common due to the prevalent use of directional laser and radar sensors. However, small UAVs may have a difficult time making accurate bearing measurements given their limited aperture and the fact that they are much more sensitive to wind-blown disturbances. Moreover, power constraints on small UAVs limit the range and strength of their radar transmissions.

Other papers have focused on static sensors that are capable of toggling between active and resting states [15]–[19] or by arranging the scheduling and reporting of measurements in an optimal manner [20], [21]. The placement of static sensor nodes for tracking in an underwater scenario is investigated in [3], [22], [23]. The advantages of mobile sensors are studied in [6], [24], where sensors are constrained to remain in small groups that retain observability of the target states. The motion and geometric formation effects of these groups on tracking performance are then investigated. In [25], the optimal positions of a set of UAVs in a tracking scenario are determined based on the Cramér-Rao bound. These results provide insight into the relationship between the angular distribution of the UAV team and target state estimation using range, range-rate, and bearing measurements. However, the results are derived under the assumption that the accuracy of the UAV measurements are constant, and not a function of the relative position of the UAVs and the target. In addition, the solution proposed in [25] provides an optimal set of UAV positions, but no path planning for the UAVs is provided, nor are there any guarantees that the resulting positions are feasible for the dynamically constrained UAVs to reach in the allotted time.

In this work, we assume a multistatic radar scenario in which a transmitter, either airborne or on the ground, illuminates a target with a radar signal. A team of UAVs receives the target reflection, and each UAV makes a local time-delay and Doppler measurement. These measurements are then sent to a centralized processor or base which uses this collected data set to track the target's position and velocity. Based on the calculated accuracy of the tracking algorithm, the base determines trajectories for the UAV team in order to optimize performance, and sends heading commands to the UAVs to best position them for the next measurement. The maneuverability of the UAVs provides the base with the ability to improve tracking performance through the tunable parameters in the tracking algorithm. We present two general optimization algorithms for the problem, and a simpler "closed-form" solution that is considerably simpler to implement, but performs essentially as well as the optimal approaches in many situations.

The format of the paper is as follows: In Section II we describe the problem set-up, the assumed dynamic models, and relevant aspects of the Extended Kalman Filter (EKF). The issue of range-dependent measurement accuracy is also addressed. In Section III-A and III-B, two algorithms for determining the optimal UAV heading angles based on the EKF updates are presented. A more computationally efficient approach is described in Section III-C, based on heuristic observations of one of the algorithms in simple scenarios. Simulation results are presented in Section IV, and some conclusions are drawn in Section V.

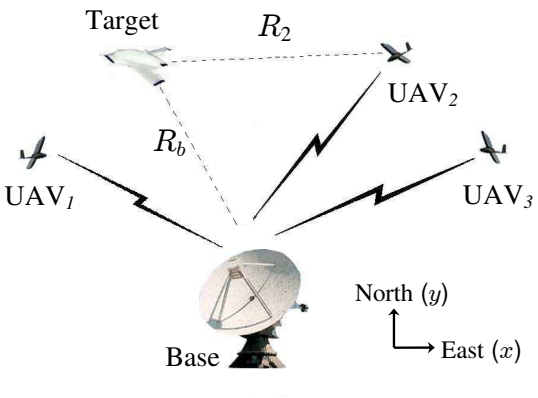

Fig. 1. Multiple UAVs tracking a single target.

II. Background and System Definition

A. Problem Statement

As illustrated in Figure 1, we consider a multistatic radar problem in which a set of N UAVs receives the signal reflected by an airborne target illuminated by a base transmitter. We assume that the UAVs are able to form time delay (τ_i) and Doppler (f_i) estimates based on these signals[1], and transmit these measurements back to the base.

The UAVs are assumed to be capable of velocity and altitude hold with an auto-pilot such as the one described in [26]. Therefore, for simplicity, we consider only a two-dimensional scenario. We define the position of the base station as the origin for our (x, y) coordinate system where x and y correspond to the cardinal directions east and north respectively. Let x, y, V_x, and V_y represent respectively the position of the target and the components of the target velocity vector in the (x, y) directions. Similarly, let x_i and y_i denote the position of the i^{th} UAV, and assume that each UAV is flying at the same constant speed V, with heading angle ψ_i measured counterclockwise from the x-axis. According to [27] and after appropriate scaling, the time-delay and Doppler measurements can be written as:

$$\tau_i = \frac{1}{c}\left(\sqrt{x^2+y^2} + \sqrt{(x-x_i)^2+(y-y_i)^2}\right) \tag{1}$$

$$f_i = \frac{1}{\lambda}\left(\frac{V_x x + V_y y}{\sqrt{x^2+y^2}} + \frac{V_p}{\sqrt{(x-x_i)^2+(y-y_i)^2}}\right) \tag{2}$$

where

$$V_p = (V_x - V\cos\psi_i)(x-x_i) + (V_y - V\sin\psi_i)(y-y_i)\ .$$

In the above equation, c and λ stand for the speed of light and the wavelength of the signal respectively.

The problem we address in this paper is how the mobility of the UAV receivers can be exploited to improve the tracking performance of the system. In our solution to this problem, the time-delay and Doppler estimates collected

[1]Another possible model would be to use time difference of arrival rather than absolute time delay. Under this model, the control algorithms developed later would remain unchanged since the observation Jacobians with respect to target parameters are identical for both models.

by the UAV team are uploaded to the base and used as measurement updates in an EKF tracking the target. Simultaneously, optimal heading commands for each UAV are calculated at the base station and then transmitted to the agents. The precise optimality criteria used for computing the heading commands will be presented in Section III.

B. UAV Receivers and Measurement Error

The accuracy of the UAV measurements is a function of the transmitted radar signal, the signal strength, the length of the propagation path from transmitter to receiver, and so on. To quantify the time-delay and Doppler measurement accuracy for UAV i, we use the Cramér-Rao Bound (CRB):

$$\mathrm{CRB}_i \leq \mathcal{E}\left[\begin{array}{c} \hat{\omega}_i - \omega_i \\ \hat{\tau}_i - \tau_i \end{array}\right] \left[\hat{\omega}_i - \omega_i \; \hat{\tau}_i - \tau_i\right] \; , \tag{3}$$

where $\mathcal{E}$ denotes the expected value, and $\hat{\omega}_i - \omega_i \; \hat{\tau}_i - \tau_i$ represent the Doppler and time delay estimation error for UAV i. As derived in [28], the CRB can be expressed as

$$\mathrm{CRB}_i^{-1} = \frac{2E_r}{N_0}\left(\frac{E_r}{E_r + N_0}\right)\left[\begin{array}{cc} \overline{\omega^2} & \overline{\omega t} \\ \overline{\omega t} & \overline{t^2} \end{array}\right] \; , \tag{4}$$

where

$$\begin{aligned} \overline{\omega^2} &= \frac{1}{2\pi}\int_{-\infty}^{\infty} \omega^2 \left|\tilde{S}(j\omega)\right|^2 d\omega \\ \overline{\omega t} &= \mathbf{Im}\int_{-\infty}^{\infty} u\tilde{s}(u)\frac{\partial \tilde{s}^*(u)}{\partial u} du \\ \overline{t^2} &= \int_{-\infty}^{\infty} u^2 \left|\tilde{s}(u)\right|^2 du \\ \omega_i &= 2\pi f_i \; , \end{aligned}$$

$\tilde{s}(u)$ and $\tilde{S}(j\omega)$ are respectively the complex envelope of the transmitted signal and its Fourier transform, **Im** represents the imaginary part of its argument, E_r is the average received signal power and $\frac{N_0}{2}$ is the spectral density of the white bandpass Gaussian noise from the receiver on each UAV. Inverting (3) yields the following explicit expression for the CRB:

$$\mathrm{CRB}_i = \frac{N_0(E_r + N_0)}{2E_r^2\left[\overline{\omega^2}\;\overline{t^2} - (\overline{\omega t})^2\right]}\left[\begin{array}{cc} \overline{t^2} & -\overline{\omega t} \\ -\overline{\omega t} & \overline{\omega^2} \end{array}\right] . \tag{5}$$

The accuracy of the second step, finding the position and velocity estimates for the target from the time-delay and Doppler estimates, is quantified in the next section by the EKF. This is done through a Jacobian that maps the accuracy of the time-delay and Doppler estimates to the position and velocity of the target. We will use the standard bistatic radar equation [29] to model the received signal power E_r [30], based on the geometry of the bistatic radar scenario depicted in Figure 2:

$$E_r = \frac{E_t G_t G_r \lambda^2 \sigma_b}{(4\pi)^3 R_b^2 R_i^2}, \tag{6}$$

where E_t is the transmit power, G_t, G_r are antenna gains at the base station and UAV side respectively, λ is the wavelength of the transmitted radio signal, and σ_b is the Radar Cross Section (RCS) of the target.

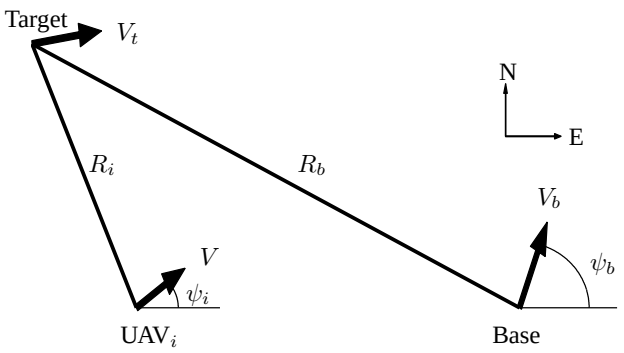

Fig. 2. Bistatic Radar Scenario.

C. Extended Kalman Filter

The need for the EKF is apparent from the nonlinear measurement equations in (1) and (2). We represent the target state vector at time k as $\mathbf{x}_k = [x\ y\ V_x\ V_y]^T$, and define the vector $\mathbf{h}_k(\mathbf{x}_k)$ to indicate the relationships in (1) and (2) that relate target position and velocity to the exact time-delay and Doppler at each UAV:

$$\mathbf{h}_k(\mathbf{x}_k) \triangleq [\tau_1\ \ldots\ \tau_N\ f_1\ \ldots\ f_N]^T$$

where, as defined earlier, N is the number of UAV receivers. Assuming that the target motion can be described by a linear discrete-time system, and assuming that the UAV measurements of time-delay and Doppler are subject to measurement noise, the system model can be written as

$$\mathbf{x}_k = \mathbf{A}_k\mathbf{x}_{k-1} + \boldsymbol{\omega}_{k-1} \tag{7}$$

$$\mathbf{z}_k = \mathbf{h}_k(\mathbf{x}_k) + \boldsymbol{\nu}_k\ , \tag{8}$$

where $\mathbf{A}_k$ is the state transition matrix, and $\boldsymbol{\omega}_{k-1} \sim \mathcal{N}(\mathbf{0}, \mathbf{Q}_{k-1})$ and $\boldsymbol{\nu}_k \sim \mathcal{N}(\mathbf{0}, \mathbf{R}_k)$ are respectively the process and measurement noise, which are assumed to be uncorrelated zero-mean Gaussian random vectors with covariances $\mathbf{Q}_k$ and $\mathbf{R}_k$.

As with the standard Kalman filter, the EKF can be divided into two stages: the time update and measurement update steps. With the time update, we propagate the target's state estimate and prediction covariance matrix as

$$\hat{\mathbf{x}}_k^- = \mathbf{A}_k\hat{\mathbf{x}}_{k-1} \tag{9}$$

$$\mathbf{P}_k^- = \mathbf{A}_k\mathbf{P}_{k-1}\mathbf{A}_k^T + \mathbf{Q}_{k-1}\ . \tag{10}$$

Once we have the measurements from the sensors, we update our estimate as:

$$\hat{\mathbf{x}}_k = \hat{\mathbf{x}}_k^- + \mathbf{K}_k(\mathbf{z}_k - \mathbf{h}_k(\hat{\mathbf{x}}_k^-)) \tag{11}$$

$$\mathbf{P}_k = (\mathbf{I} - \mathbf{K}_k\mathbf{H}_k)\mathbf{P}_k^- \tag{12}$$

where

$$\mathbf{K}_k = \mathbf{P}_k^- \mathbf{H}_k^T (\mathbf{H}_k \mathbf{P}_k^- \mathbf{H}_k^T + \mathbf{R}_k)^{-1} \,. \tag{13}$$

In the above equations, $\mathbf{H}_k = (\frac{\partial \mathbf{h}_k}{\partial \mathbf{x}})^T$ is a function of the UAVs' positions and headings.

The basic idea of this paper will be to reduce the "size" of the estimation error by updating the heading of the UAVs, and hence $\mathbf{H}_k$. In essence, we are applying an outer control loop around the Kalman filter.

D. System Dynamics

The approach presented in the next section is general enough to accommodate any particular model for $\mathbf{A}_k, \mathbf{Q}_k$ or $\mathbf{R}_k$. In the simulation studies presented later, we will assume a simple constant velocity target model, described by the state transition matrix

$$\mathbf{A}_k = \begin{bmatrix} 1 & 0 & \Delta_t & 0 \\ 0 & 1 & 0 & \Delta_t \\ 0 & 0 & 1 & 0 \\ 0 & 0 & 0 & 1 \end{bmatrix} , \tag{14}$$

where Δ_t is the time interval between samples. We will also use a simple white process noise model:

$$\mathbf{Q}_k = \mathrm{diag}\left(\sigma_x^2, \sigma_y^2, \sigma_{V_x}^2, \sigma_{V_y}^2\right). \tag{15}$$

The definition of the measurement noise model is more critical to the problem at hand, since it will be a function of the UAV positions. Assuming that the measurement noise is uncorrelated for each UAV, the expression for the CRB derived above can be used to find the elements of $\mathbf{R}_k$. For $1 \le i \le N$,

$$\mathbf{R}_k(i,j) = E(\nu_i \nu_j^*) = \begin{cases} \mathrm{CRB}_i(1,1) & j = i \\ \frac{1}{2\pi}\mathrm{CRB}_i(1,2) & j = i+N \\ 0 & \text{elsewhere} \,. \end{cases}$$

When $N < i \le 2N$,

$$\mathbf{R}_k(i,j) = E(\nu_i \nu_j^*) = \begin{cases} (\frac{1}{2\pi})^2\mathrm{CRB}_{i-N}(2,2) & j = i \\ \frac{1}{2\pi}\mathrm{CRB}_{i-N}(2,1) & j = i-N \\ 0 & \text{elsewhere} \,. \end{cases}$$

We assume the ability of the base to pass a heading command $\psi_{i,k}$ to UAV i. Assuming an instantaneous response to heading commands, the UAVs will fly in a straight line with a velocity V and heading ψ_i during each time interval. The inertial position of UAV i after time interval k can be approximated by:

$$x_{i,k} = x_{i,k-1} + V\cos(\psi_{i,k})\Delta_t \tag{16}$$

$$y_{i,k} = y_{i,k-1} + V\sin(\psi_{i,k})\Delta_t \,. \tag{17}$$

This approximation will be valid as long as the new heading commands are not too different from the UAV's current heading and the time steps are short enough. Constraints on changes to the UAV heading will be imposed in the development of the heading algorithms in the next section.

It is well known that, due to the geometry of a bistatic radar system, the bistatic radar ambiguity function, which is an indicator of how well position and velocity can be determined from the received waveform, is a nonlinear function of the transmitter, receiver, and target positions [31]–[33]. In our approach, each UAV calculates only the time-delay and Doppler information available to it, under the assumption that the received signal can be unambiguously associated with the target being tracked. The time-delay and Doppler measurements are then passed to the base station for processing; the nonlinearities arising in the bistatic radar ambiguity function are encountered at this step when the velocity and position estimates are extracted from the measured time-delay and Doppler. These nonlinearities are accounted for through the Jacobian $\mathbf{H}_k$ in the EKF.

III. Heading Algorithms

In this section we present two algorithms for finding the optimal UAV heading commands from the EKF. In the first algorithm, the headings are chosen to minimize the weighted trace of the EKF prediction error covariance matrix one-step into the future. In the second, UAV headings are found that maximize the information provided by the measurements at the next step. A heuristic simplification of the second algorithm is also presented that leads to a closed-form solution to the problem, and considerable computational savings.

A. Error Covariance Minimization (ECM)

The motivation underlying the approach presented here is simply to fly the UAVs in directions at time $t = k$ such that the estimation error at time $t = k+1$ is made as small as possible. To this end, we minimize the weighted trace of the one-step-ahead prediction error covariance $\mathbf{P}_{k+1}^{\text{-}}$ [34]. In practical scenarios, the UAV dynamics limit the rate at which its heading may change. Therefore, for each step we restrict the UAVs' position to an arc defined by the previous heading. Mathematically, the idea is to find the vector of heading commands $\mathbf{\Psi}_k = [\psi_{1,k} \dots \psi_{N,k}]^T$ as follows:

$$\begin{aligned} \mathbf{\Psi}_k &= \arg\min_{\mathbf{\Psi}_k} tr(\mathbf{W}_k \mathbf{P}_{k+1}^{\text{-}}) \\ |\psi_{i,k} - \psi_{i,k-1}| &\leq C \ \ \forall \ \ i = 1 \dots N \,, \end{aligned} \tag{18}$$

where $\mathbf{W}_k$ is a positive semi-definite weighting matrix and C is the upper bound on the turning rate of the UAVs. The weighting matrix $\mathbf{W}_k$ is used to account for the fact that the units of the elements of the covariance matrix are different, and to allow one to emphasize the need for greater accuracy for certain parameters and in certain dimensions.

Replacing $\mathbf{P}_{k+1}^{\text{-}}$ in (18) with the expressions in (10) and (12) yields

$$tr\left(\mathbf{W}_k \mathbf{A}_{k+1} [(\mathbf{P}_k^{\text{-}})^{-1} + \mathbf{H}_k^T \mathbf{R}_k^{-1} \mathbf{H}_k]^{-1} \mathbf{A}_{k+1}^T + \mathbf{W}_k \mathbf{Q}_k\right) \ . \tag{19}$$

Since the dependence of the cost function on the UAV headings is not explicit, it is useful to examine the optimization problem in slightly more detail. Equation (18) depends on the heading angles through $\mathbf{H}_k$ and $\mathbf{R}_k$ in equation (19), which in turn depend on the positions of the UAVs at time k, which are a function of their positions at time $k-1$ and the heading angles chosen at time $k-1$ (as described by the model in Eqs. (16) and (17)). Thus, when we minimize (18) with respect to Ψ_k, we are minimizing it with respect to the headings chosen at time $k-1$ after the measurement at time $k-1$, which are also the headings in force at time k before measurement k is taken.

When the number of UAVs is not too large, a finite grid search can be used to optimize the cost function. For higher dimensional problems, we employ a Quasi-Newton approach to minimize (19). At each iteration the heading is updated by $\mathbf{\Psi}_{m+1} = \mathbf{\Psi}_m - \mathbf{S}_m^{-1}\mathbf{g}_m$, where $\mathbf{S}_m^{-1}$ and $\mathbf{g}_m$ are the Hessian matrix and gradient vector of the cost function evaluated at $\mathbf{\Psi}_m$. Due to the complexity involved in calculating the Hessian matrix, the Quasi-Newton approach uses an estimate of the Hessian based on the gradient vector. The gradient with respect to the heading of the i^{th} UAV at time k is given by

$$\frac{\partial tr(\mathbf{W}_k\mathbf{P}_{k+1}^{\text{-}})}{\partial \psi_{i,k}} = -tr\left(\mathbf{W}_k\mathbf{A}_{k+1}\mathbf{B}^{-1}\frac{\partial \mathbf{B}}{\partial \psi_{i,k}}\mathbf{B}^{-1}\mathbf{A}_{k+1}^T\right) , \tag{20}$$

where

$$\begin{aligned}\mathbf{B} &= (\mathbf{P}_k^{\text{-}})^{-1} + \mathbf{H}_k^T\mathbf{R}_k^{-1}\mathbf{H}_k \\ \frac{\partial \mathbf{B}}{\partial \psi_{i,k}} &= \frac{\partial \mathbf{H}_k^T}{\partial \psi_{i,k}}\mathbf{R}_k^{-1}\mathbf{H}_k + \left(\frac{\partial \mathbf{H}_k^T}{\partial \psi_{i,k}}\mathbf{R}_k^{-1}\mathbf{H}_k\right)^T - \mathbf{H}_k^T\mathbf{R}_k^{-1}\frac{\partial \mathbf{R}_k}{\partial \psi_{i,k}}\mathbf{R}_k^{-1}\mathbf{H}_k .\end{aligned}$$

The problem boils down to calculating $\frac{\partial \mathbf{H}_k}{\partial \psi_{i,k}}$ and $\frac{\partial \mathbf{R}_k}{\partial \psi_{i,k}}$, where $\mathbf{H}_k$ is $2N \times 4$ and $\mathbf{R}_k$ is $2N \times 2N$. Minimizing the cost function (18) over the correct control variable will work generally for any adaptive sensor network.

B. Maximizing Information (MI)

We investigate here an alternative approach based on the use of the so-called information matrix (or inverse covariance matrix) as the defining metric for tracking performance. Intuitively, the information matrix is a measure of the amount of information about the parameters of interest contained in the observations. There are two key reasons for using the information matrix in this context. The first is the computational savings that result due to the simpler form of the information matrix measurement update. Second, the UAV heading parameters enter into the information matrix update in a much simpler way that lends itself more easily to approximation. A "closed-form" solution based on such an approximation is presented in the next section. A computationally efficient optimization method was found in [9] for a similar application that used the trace of the covariance matrix, but it was for a much simpler measurement model than assumed here.

As in [2], in our approach we maximize the determinant of the *new information* contained in the measurements to determine the optimal heading commands for the UAV team [35]. The information matrix update can be found by applying the matrix inversion lemma to the covariance measurement update in Equation (12), yielding

$$\mathbf{P}_k^{-1} = (\mathbf{P}_k^{\text{-}})^{-1} + \mathbf{H}_k^T\mathbf{R}_k^{-1}\mathbf{H}_k , \tag{21}$$

where $\mathbf{P}_k^{-1}$ is the information matrix. The term $\mathbf{H}_k^T\mathbf{R}_k^{-1}\mathbf{H}_k$ is the new information contained in the measurements $\mathbf{z}_k$; it is this term whose influence we wish to maximize. Since $\mathbf{H}_k$ enters into the update quadratically, an analysis of the impact of the UAV headings is much simpler. As discussed in the next section, this allows for the development of a computationally efficient algorithm for computing the optimal heading commands.

In this approach, the heading commands are found by solving

$$\begin{aligned} \Psi_k &= \arg\max_{\Psi_k} \det\,(\mathbf{H}_k^T\mathbf{R}_k^{-1}\mathbf{H}_k) \\ |\psi_{i,k} - \psi_{i,k-1}| &\leq C \;\; \forall \;\; i = 1 \ldots N\,. \end{aligned} \tag{22}$$

Assuming the measurements from each UAV are uncorrelated, after regrouping the time-delay and Doppler equation vector as $\mathbf{h}_k(x_k) = [\tau_1 \;\; f_1 \;\; \ldots \;\; \tau_N \;\; f_N]^T$, the covariance matrix $\mathbf{R}_k$ will have a block diagonal structure. Each block along the diagonal is denoted by $\mathbf{R}_k^i$, which is equivalent to the CRB matrix discussed in Section II-B. More algebraic manipulation leads to the following equality:

$$\begin{aligned} \varphi_k \triangleq \mathbf{H}_k^T\mathbf{R}_k^{-1}\mathbf{H}_k &= \sum_{i=1}^{N} \mathbf{H}_k^{iT}(\mathbf{R}_k^i)^{-1}\mathbf{H}_k^i \\ \mathbf{H}_k^T &= [\mathbf{H}_k^{1T} \ldots \mathbf{H}_k^{NT}]\,. \end{aligned} \tag{23}$$

The sub-matrices, $\mathbf{H}_k^i$, which constitute the measurement gradient matrix, $\mathbf{H}_k^T$, are defined in Equation (35) of the Appendix.

C. Approximate Closed-Form Solution (MIA)

In the Appendix, it is shown that if the relative positions of the UAVs and target do not dramatically change over one time step, then the cost function $J(\mathbf{\Psi}_k) = \det\,\varphi_k$ in (22) can be approximately decoupled as

$$\begin{aligned} J(\psi_{i,k}) = \alpha_{i,1}^k \sin(\psi_{i,k} + \theta_{i,1}^k) + \\ \alpha_{i,2}^k \sin(2\psi_{i,k} + \theta_{i,2}^k) + \beta_{i,k} + n(i,k), \end{aligned} \tag{24}$$

where $\alpha_{i,m}^k, \theta_{i,m}^k, \beta_{i,k}, m = 1, 2$ are unknown and independent of $\psi_{i,k}$, $n(i,k)$ accounts for approximation error, and only $\beta_{i,k}$ depends on the headings of the other UAVs. Based on this observation, we propose a sequential optimization approach that maximizes (24) one UAV at a time, while holding the heading of the others fixed.

Values for $\alpha_{i,1}^k, \alpha_{i,2}^k, \theta_{i,1}^k$ and $\theta_{i,2}^k$ are found by fitting (24) to samples of the criterion function $J(\psi)$. In particular, treating the approximation error as Gaussian, the following maximum likelihood estimators of the unknown parameters can be formulated:

$$\begin{aligned} \hat{\theta}_{i,m}^k &= \arctan\left(\frac{\int_0^{2\pi} J(t_1)\cos(mt_1)dt_1}{\int_0^{2\pi} J(t_2)\sin(mt_2)dt_2}\right) \\ \hat{\alpha}_{i,m}^k &= \arctan\left(\frac{\int_0^{2\pi} J(t_1)\sin(mt_1 + \hat{\theta}_{i,m}^k)dt_1}{\int_0^{2\pi} \sin^2(mt_2 + \hat{\theta}_{i,m}^k)dt_2}\right)\,. \end{aligned} \tag{25}$$

In practice, the integrals in (25) are numerically evaluated by calculating the cost function at $\psi_{i,k} = [0, \frac{1}{L}2\pi, \ldots, \frac{L-1}{L}2\pi]$ and assigning all other UAVs their previous heading at the last iteration. In the simulations presented later, $L = 10$ sample headings were used.

Once the amplitudes and phases are estimated, setting the derivative of the cost function $J(\psi_{i,k})$ with respect to $\psi_{i,k}$ to be zero leads to the following fourth-order polynomial equation in x:

$$\left(4\alpha_{i,2}^k \cos\theta_{i,2}^k x^2 + \alpha_{i,1}^k \cos\theta_{i,1}^k x - 2\alpha_{i,2}^k \cos\theta_{i,2}^k\right)^2 = \left(4\alpha_{i,2}^k \sin\theta_{i,2}^k x + \alpha_{i,1}^k \sin\theta_{i,1}^k\right)^2 (1 - x^2) \tag{26}$$

Real-valued solutions x within the unit circle correspond to candidate optimal headings through the relationship $\cos\psi_{i,k} = x$. If multiple candidate solutions exist within the UAV turning radius, the one which leads to the largest value for $J(\psi_{i,k})$ is chosen. Real-valued solutions outside the turning radius are evaluated at the nearest boundary point. If there are no real-valued solutions inside the unit circle, $J(\psi_{i,k})$ is evaluated at the current heading and at the boundaries of the feasible region, and the heading that results in the largest value is chosen. The above process is repeated for each UAV and iterated across the UAV team until the resulting performance gain is negligible.

IV. Simulation Results

A. Simulation Setup

As discussed in Section II-B, the accuracy of the measurements can be adjusted by configuring the various transmitted signal parameters. A close look at (5) reveals that the CRB for time delay and Doppler shift can be decoupled if the transmitted baseband signal is real. In our simulations, we assume a train of Gaussian-shaped pulses as the transmitted signal, in which case the CRB matrix will assume a diagonal structure. The complex envelope of the signal is expressed as

$$\tilde{s}(t) = \frac{1}{\sqrt{2N_p+1}} \left(\frac{\sigma^2}{\pi}\right)^{\frac{1}{4}} \sum_{k=-N_p}^{N_p} e^{-\frac{\sigma^2(t-kT)^2}{2}}, \tag{27}$$

where T is the Inter-Pulse Period (IPP), σ is a parameter that controls the effective duration of each Gaussian pulse, and $2N_p + 1$ is the number of Gaussian pulses that compose the transmitted signal.

The choice of the transmitted pulse impacts the quality of the time delay and Doppler estimates, which must be quantified in order to specify the measurement covariance matrix $\mathbf{R}_k$ for each UAV. For the Gaussian pulse train considered here, it can be shown that $\overline{\omega t} = 0$. Under the assumption that $T \gg \frac{1}{\sigma}$, $\overline{t^2}$ can be approximated as $\frac{N_p(N_p+1)}{3}T^2$, and the CRB for the Doppler estimate can be found from (3)-(5) to be

$$\mathrm{Var}\left(\hat{f} - f\right) \geq \left(\frac{1}{2\pi}\right)^2 \left[\frac{2Er}{N_0}\left(\frac{Er}{Er+N_0}\right)\right]^{-1} \left(\overline{t^2}\right)^{-1} . \tag{28}$$

Similarly, for the time-delay estimate,

$$\mathrm{Var}\left(\hat{\tau} - \tau\right) \geq \left[\frac{2Er}{N_0}\left(\frac{Er}{Er+N_0}\right)\right]^{-1} \left(\overline{\omega^2}\right)^{-1} \tag{29}$$

$$\overline{\omega^2} = \frac{1}{(2N_p+1)\sqrt{\pi}\sigma} \int_{-\infty}^{\infty} \omega^2 e^{-\frac{\omega^2}{\sigma^2}} \left(\frac{\sin\frac{2N_p+1}{2}\omega t}{\sin\frac{\omega t}{2}}\right)^2 d\omega .$$

While numerical integration can be carried out to evaluate this expression, for simplicity we use the following loose bound to model the time-delay estimation accuracy:

$$\mathrm{Var}\left(\hat{\tau}-\tau\right) > \left[\frac{2Er}{N_0}\left(\frac{Er}{Er+N_0}\right)\right]^{-1}\frac{2}{(2N_p+1)\sigma^2}\ . \tag{30}$$

Other signal designs for the transmit signal are available in the literature [36], [37].

In the following simulations, we simulate a simple scenario involving 2 UAVs tracking a moving target. We assume an average transmit power of 15 watts at the Base Station (BS) located at the origin, a carrier frequency of $f_0 = 10$ GHz, number of transmitted pulses $N_p = 31$, an IPP of $T = 1$ ms, receive noise figure $F = 5$ dB, noise reference temperature $T_0 = 290$ K, and Gaussian pulse parameter $\sigma = 10^5$ Hz. The algorithm updates its estimate once every second, and the heading change constraint C in (18) is set to be $\frac{\pi}{9}$.

The initial coordinates of the UAVs were assumed to be $(10, -20)$km and $(10, -10)$km. Both of the UAVs are given initial headings of 0°, and the simulation was run for 1500s. The UAVs move with constant speed $80\sqrt{2}$ m/s. The target's initial location and speed were $(0, 50)$km and 100 m/s, respectively. Its initial heading was randomly generated for each simulation, and for the results presented in the figures below it was about -85°. The target's RCS is assumed to be $\sigma_b = 100\mathrm{m}^2$ and its trajectory is generated according to (7). For the Kalman Filter, we set the initial state estimate to be the true target location, and the covariance matrix associated with the initial position to be the identity matrix. The process covariance matrix was set to be $\mathbf{Q}_k = \mathrm{diag}(50, 50, 3, 3)$, and the time-varying measurement covariance matrix $\mathbf{R}_k$ was generated according to the model described in Section II-D. The antenna gains at the BS side and the UAV side were assumed to be 40 dB and 30 dB respectively.

B. Results

We present results for a two-agent UAV team tracking a maneuvering target. Results for five UAV heading update algorithms are presented: the error covariance minimization (ECM) approach of (18), information maximization (MI) according to (22), the approximate solution (MIA) described in the previous section, random UAV headings, and fixed UAV positions.

In Figures 3-5, we plot the performance of the error covariance minimization approach of (18). The trajectories of each UAV and the target are shown in Fig. 3; the starting postions are denoted by crosses (likewise for all subsequent trajectory plots). The asterisks on each trajectory indicate the UAV and target positions at 300 second time intervals, so that the relative motion of the platforms can be observed. The heading angles for each UAV are plotted in Fig. 4. Note that although the initial heading of UAV-1 was 0°, it almost immediately reverses course to a heading of 180°. The UAVs generally tend to follow the target due to the system's desire to increase the SNR (reduce path loss), while at the same time spreading out in order to improve resolution of the target position and dynamics. Fig. 5 shows the norm of one run of the actual tracking error for both the position and velocity estimates. Similar results are shown for the max-information algorithm in Figures 6-8. The motion of the UAVs for both algorithms is very similar, and both approaches provide similar tracking error performance.

Figures 9-11 show the results obtained by the simplified solution presented in the previous section. As observed, the UAV team behaves almost identically to the max-information approach, which shows the approximation and decoupling work well for this scenario regardless of the small number of samples used for the sinusoidal approximation ($L = 10$ as mentioned in Section III-C). The simulation run time in Matlab on a 2.16 GHz Intel Core 2 Duo processor shows that the MIA method is at least 20 times faster than the brute force MI algorithm for this specific case. For cases involving more UAVs, the savings will be even more significant. The tracking error of all of the above algorithms is considerably better than that obtained using random UAV motion (subject to the given turning constraint), as illustrated in Figures 12-13. Figure 14 shows the norm of the actual tracking error for one run of a scenario with sensors fixed at the initial UAV locations. Much larger tracking errors are observed in this case. This is due to the relatively small aperture of the sensing array formed by the two UAVs, and its poor orientation relative to the targe. Clearly, the use of closed-loop heading control significantly reduces the tracking error by arranging the UAVs into a more optimal orientation.

It is clear from the examples above that there are two competing factors that drive the behavior of the mobile UAV sensors: (1) the desire to reduce the range to the target in order to keep the received signal power from becoming too small, and (2) the need for the sensors to spread out and provide a larger aperture for localization. All three of the algorithms provide an automated way of balancing these competing objectives. Initially, the UAVs spread apart and move towards the target. As the target passes, they reverse course, but because of the turning radius constraint and their current headings, they turn towards each other instead of spreading out. One reason for this behavior is that the proposed algorithm is somewhat myopic, looking only one time step ahead. An approach that attempted to predict the target location at some time farther in the future may be able to sacrifice a short-term performance gain for a smaller long-term tracking error. This is the subject of on-going research.

V. Conclusions

In this paper, we have presented several methods for controlling the movement of mobile sensor platforms in order to improve target tracking performance. Two optimization criteria were derived for the problem, both of which require some type of search procedure in order to find the desired solution. Simulations were used to show the benefit of using closed-loop sensor control for the special case of an EKF tracking filter. In addition, a simpler closed-form approach based on one of the algorithms was also presented, and shown to have performance similar to that obtained using the optimal algorithms.

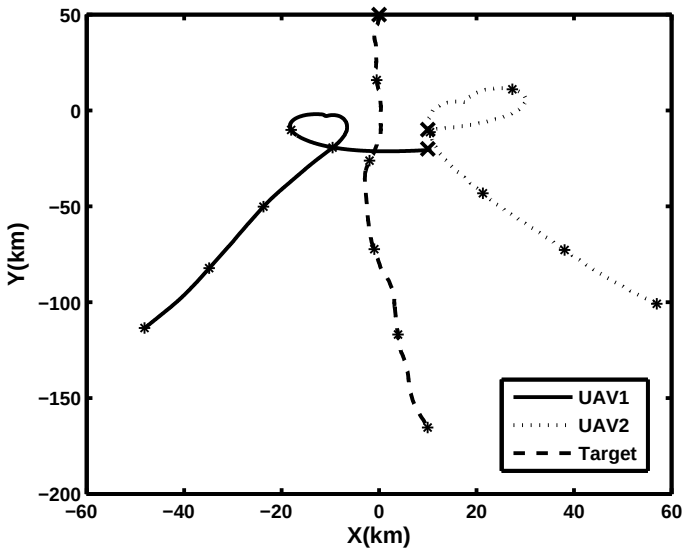

Fig. 3. Trajectories of UAVs and target using ECM. A '*' marker has been placed on each trajectory every 300s to help visualize the time evolution.

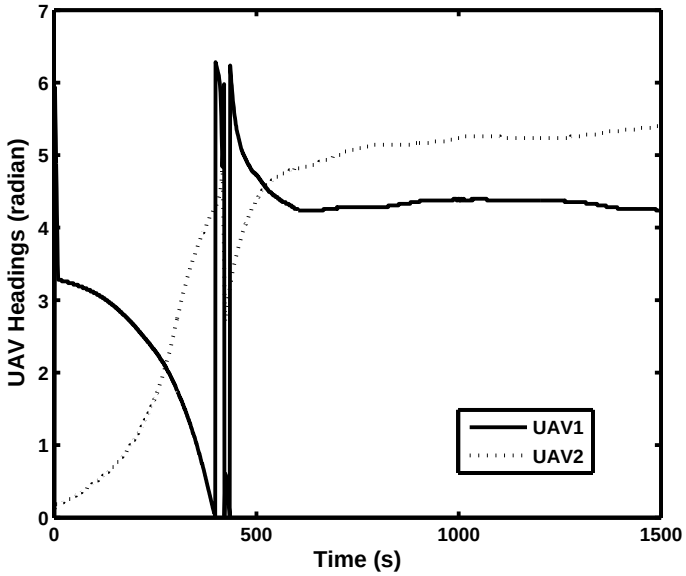

Fig. 4. UAV headings with control using ECM.

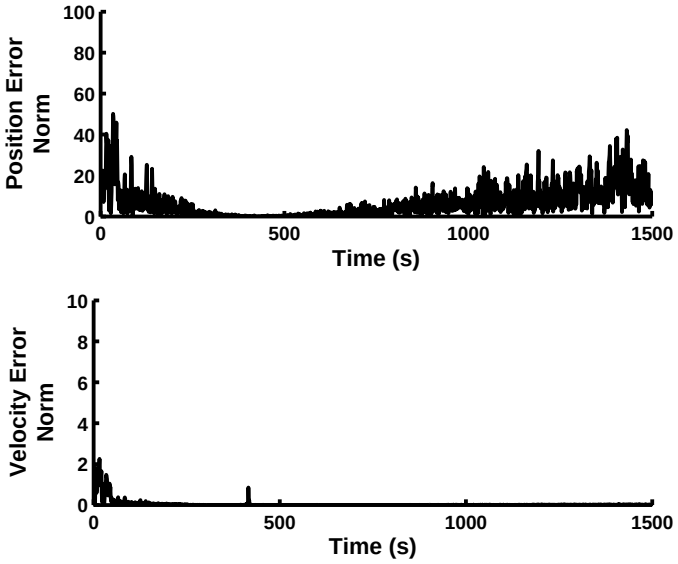

Fig. 5. Norm of tracking error using ECM.

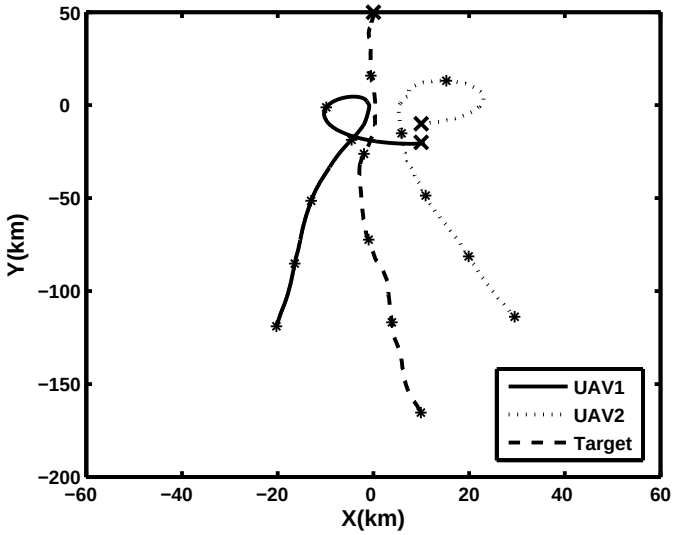

Fig. 6. Trajectories of UAVs and target using MI. A '*' marker has been placed on each trajectory every 300s to help visualize the time evolution.

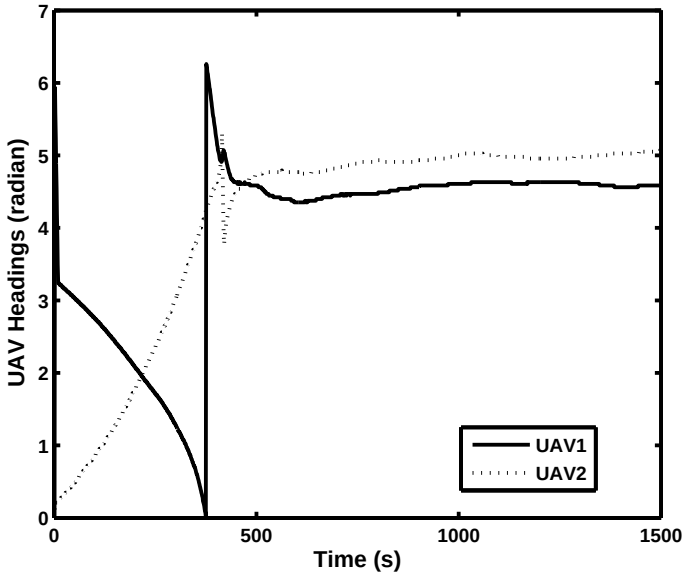

Fig. 7. UAV headings with control using MI.

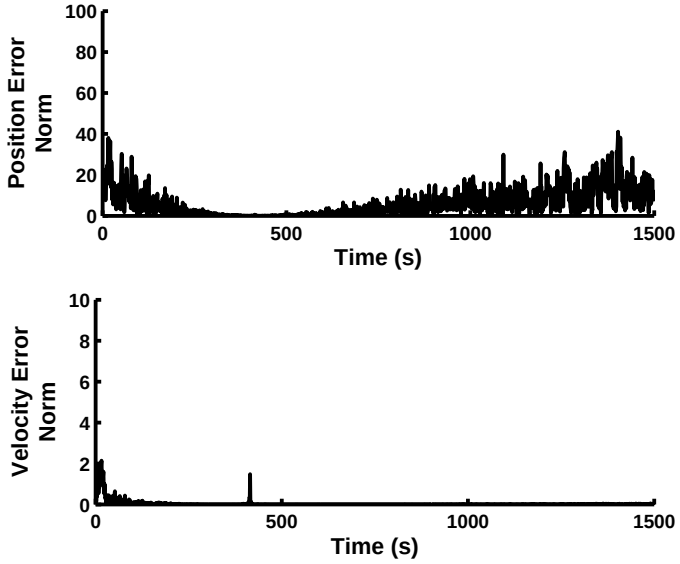

Fig. 8. Norm of tracking error using MI.

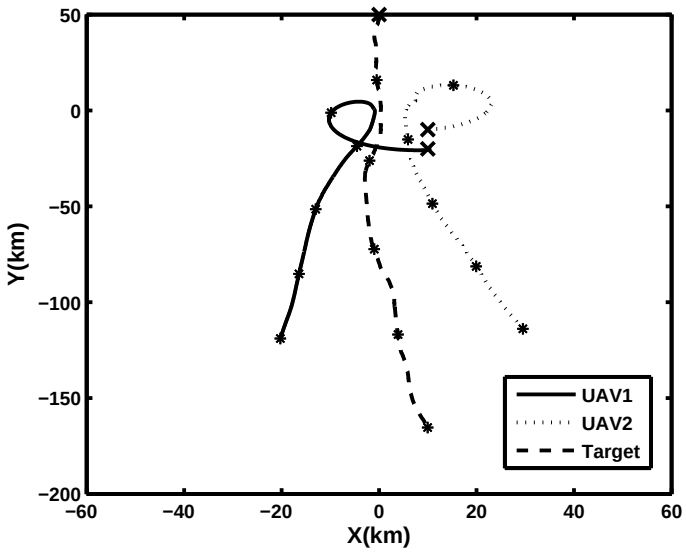

Fig. 9. Trajectories of UAVs and target using MIA. A '*' marker has been placed on each trajectory every 300s to help visualize the time evolution.

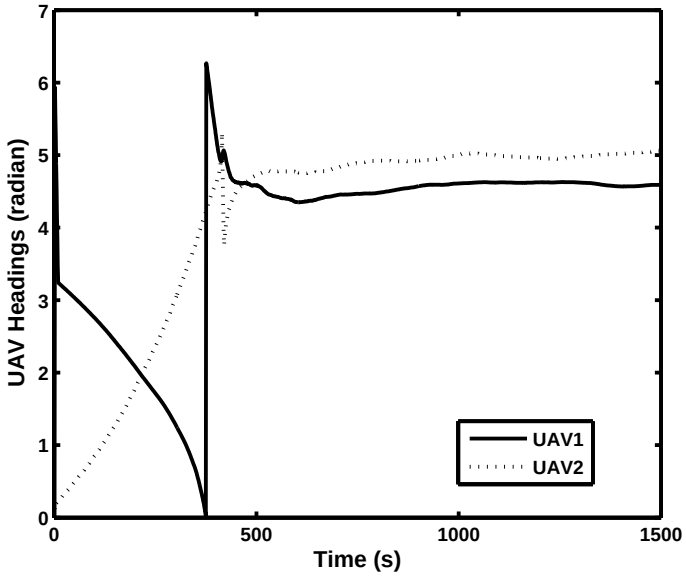

Fig. 10. UAV headings using MIA.

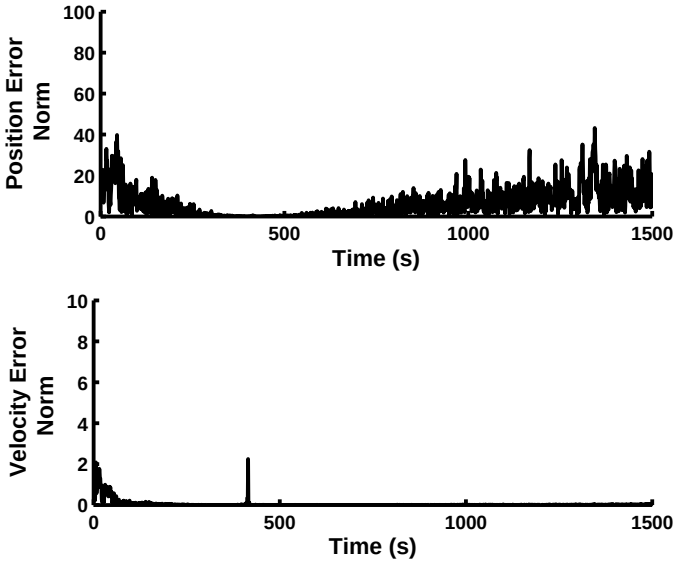

Fig. 11. Norm of tracking error using MIA.

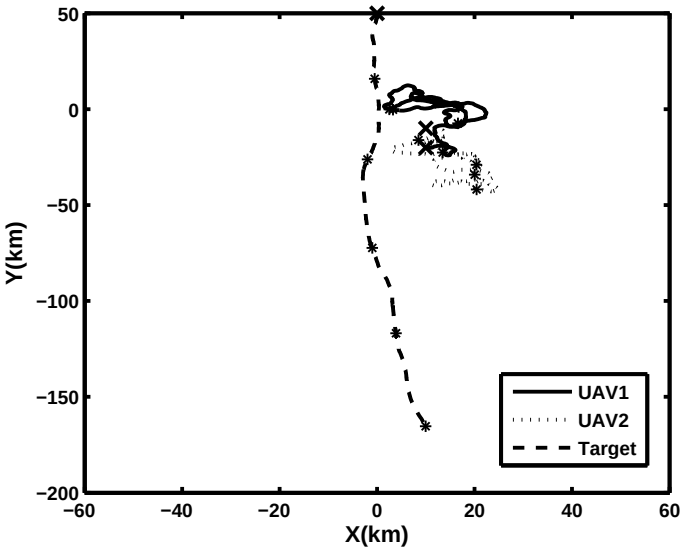

Fig. 12. Trajectories of UAVs and target with random headings. A '*' marker has been placed on each trajectory every 300s to help visualize the time evolution.

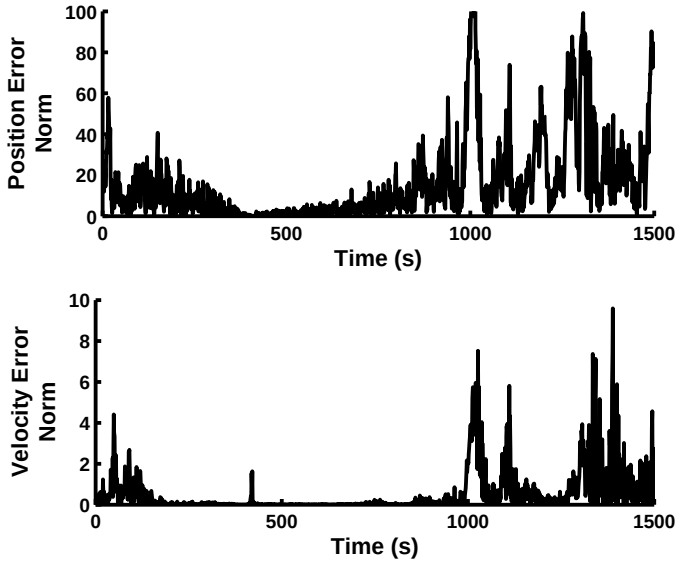

Fig. 13. Norm of tracking error with random headings.

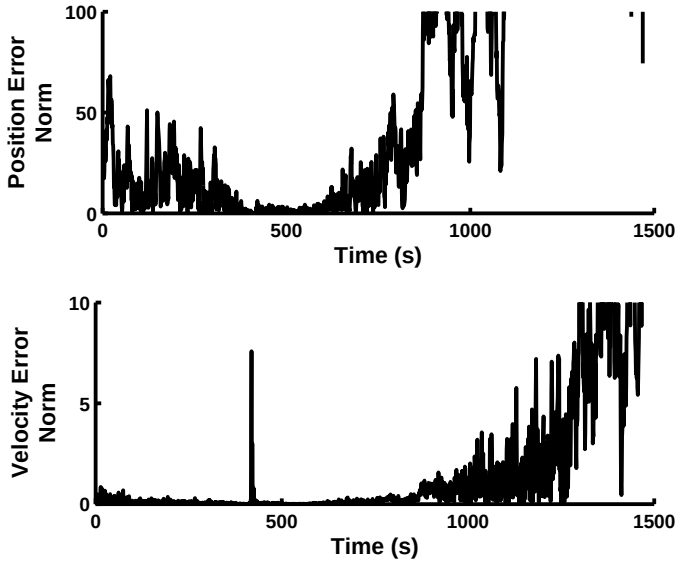

Fig. 14. Norm of tracking error with fixed-position sensors.

VI. APPENDIX

This appendix provides justification for the approximation to the information matrix cost function in (22).

A. Time-Delay Approximation

Recalling the delay expression (1) and the UAV dynamic model in (16)-(17), we can rewrite the time-delay measurement at the i^{th} UAV at time $t = k$ as

$$\begin{aligned}
\tau_k(i) &= \frac{1}{c}\left(\sqrt{x_k^2 + y_k^2} + \sqrt{(x_k - x_{i,k})^2 + (y_k - y_{i,k})^2}\right) \\
&= \frac{1}{c}\left(\sqrt{x_k^2 + y_k^2} + \sqrt{r_{i,k}^2 - 2r_{i,k}V\Delta_t\cos(\psi_{i,k} - \theta_{i,k}) + V^2\Delta_t^2}\right) \\
r_{i,k} &= \sqrt{(x_k - x_{i,k-1})^2 + (y_k - y_{i,k-1})^2} \\
\theta_{i,k} &= \arctan\frac{y_k - y_{i,k-1}}{x_k - x_{i,k-1}} \ .
\end{aligned} \tag{31}$$

Under the reasonable assumption that the range of each UAV to the target is much larger than the distance traveled by the UAV in one time step ($r_{i,k} \gg 2V\Delta_t$), then, after dropping the quadratic term, $V^2\Delta_t^2$, we use the approximation $\sqrt{1-\gamma} \approx 1 - \frac{1}{2}\gamma$ for $\gamma \approx 0$ to show that

$$\tau_k(i) \approx \frac{1}{c}\left(\sqrt{x_k^2 + y_k^2} + r_{i,k} - V\Delta_t\cos(\psi_{i,k} - \theta_{i,k})\right) \ . \tag{32}$$

Thus, the time delay is seen to be a sinusoidal function of the heading angles $\psi_{i,k}$.

B. Doppler Shift Approximation

Inserting the UAV dynamic model (16)-(17) into the Doppler measurement model (2) yields

$$\begin{aligned}
f_k(i) = \frac{C_1}{\lambda}\Big\{&(x_{i,k-1} - \Delta_t V_x - x_k)V\cos\psi_{i,k} \\
&+ (y_{i,k-1} - \Delta_t V_y - y_k)V\sin\psi_{i,k} + C_2\Big\} \\
&+ \frac{V_x x_k + V_y y_k}{\lambda\sqrt{x_k^2 + y_k^2}}
\end{aligned} \tag{33}$$

where

$$C_1^{-1} = r_{i,k}\sqrt{1 - \frac{2V\Delta_t}{r_{i,k}}\cos\left(\psi_{i,k} - \theta_{i,k}\right) + \frac{V^2\Delta_t^2}{r_{i,k}^2}}$$

and

$$C_2 = V^2\Delta_t + V_x(x_k - x_{i,k-1}) + V_y(y_k - y_{i,k-1}) \ .$$

Again using the fact that $r_{i,k} \gg 2V\Delta_t$, we have $C_1^{-1} \approx r_{i,k}$, and hence

$$f_k(i) \approx F_{i,k} - G_{i,k}\cos\left(\psi_{i,k} - \zeta_{i,k}\right) \tag{34}$$

where

$$F_{i,k} = \frac{V_x x_k + V_y y_k}{\lambda\sqrt{x_k^2 + y_k^2}} + \frac{C_2}{\lambda r_{i,k}}$$

$$G_{i,k} = \frac{V}{r_{i,k}\lambda}\big[(\Delta_t V_x + (x_k - x_{i,k-1}))^2 + (\Delta_t V_y + (y_k - y_{i,k-1}))^2\big]^{1/2} ,$$

and

$$\zeta_{i,k} = \arctan\frac{\Delta_t V_y + (y_k - y_{i,k-1})}{\Delta_t V_x + (x_k - x_{i,k-1})} .$$

As in the case of the time delay, the Doppler shift measurement is also approximately a sinusoidal function of $\psi_{i,k}$.

C. Cost Function Approximation

Maximizing $|\mathbf{A}_{k+1}^{-T}\mathbf{H}_k^T\mathbf{R}_k^{-1}\mathbf{H}_k\mathbf{A}_{k+1}^{-1}|$ is equivalent to maximizing $|\mathbf{H}_k^T\mathbf{R}_k^{-1}\mathbf{H}_k|$ when both $\mathbf{A}_k$ and $\mathbf{H}_k^T\mathbf{R}_k^{-1}\mathbf{H}_k$ are full rank. In (23), each $\mathbf{H}_k^i$ is a 2×4 matrix with the following structure:

$$\mathbf{H}_k^i = \begin{bmatrix} \frac{\partial\tau_k^i}{\partial x_k} & \frac{\partial\tau_k^i}{\partial y_k} & 0 & 0 \\ \frac{\partial f_k^i}{\partial x_k} & \frac{\partial f_k^i}{\partial y_k} & \frac{\partial f_k^i}{\partial V_{x,k}} & \frac{\partial f_k^i}{\partial V_{y,k}} \end{bmatrix} . \tag{35}$$

It is easily seen that the gradient of the time-delay with respect to the target's position equals the gradient of the Doppler with respect to the target's velocity (*i.e.*, $\frac{\partial f_k^i}{\partial V_{x,k}} = \frac{\partial\tau_k^i}{\partial x_k}$ and $\frac{\partial f_k^i}{\partial V_{y,k}} = \frac{\partial\tau_k^i}{\partial y_k}$). Using the time-delay and Doppler approximations given in the previous two sections and under the assumptions

$$r_{i,k} \gg V\Delta_t , \qquad r_{i,k} \gg V , \qquad \text{and} \quad r_{i,k} \gg V_T \tag{36}$$

where $V_T = \sqrt{V_x^2 + V_y^2}$, each entry in $\mathbf{H}_k^i$ (except the zero terms) can be approximated by a constant plus a sinusoid with a relatively small amplitude. Assuming Δ_t is small, the second assumption $r_{i,k} \gg V$ includes the previous cases $r_{i,k} \gg V\Delta_t$ and $r_{i,k} \gg 2V\Delta_t$. Then the two assumptions $r_{i,k} \gg V$ and $r_{i,k} \gg V_T$ state respectively that the speed of the UAV and the speed of the target must be much smaller than the range of the target from the UAV. This ensures that over short time spans the bearing angle from the UAV to the target changes slowly.

From Section II-D, we recall that $\mathbf{R}_k^i$ is a constant matrix scaled by $\frac{N_0(N_0+E_r)}{2E_r^2}$. When the SNR is not too small, i.e. $Er \gg N_0$, $(\mathbf{R}_k^i)^{-1}$ can be approximated as a constant matrix scaled by $2 \cdot \mathrm{SNR}$. Since E_r is inversely proportional to the square of $r_{i,k} - V\Delta_t\cos(\psi_{i,k} - \theta_{i,k})$, a first-order Taylor's expansion around $r_{i,k}$ can be used to show that the SNR can be approximated as a sinusoid with a constant offset that is much larger in magnitude. Let $\varphi_{i,k} \triangleq \mathbf{H}_k^{iT}(\mathbf{R}_k^i)^{-1}\mathbf{H}_k^i$. Each entry of $\varphi_{i,k}$ is the product of three sinusoids with identical harmonics ($\psi_{i,k}$) and differing phases plus constant terms that are large relative to the magnitude of the sinusoids. Thus the (j,l) entry of $\varphi_{i,k}$ can be approximated as follows:

$$\begin{aligned} \varphi_{i,k}(j,l) &\approx \sum_{m=1}^{3} a_{m,k}^i(j,l)\sin\left(m\cdot\psi_{i,k} + \phi_m(j,l)\right) + b_k^i(j,l) \\ a_{p,k}^i(j,l) &\gg a_{q,k}^i(j,l), \qquad \text{if } p < q \\ b_k^i(j,l) &\gg a_{m,k}^i(j,l), \qquad 1 \le m \le 3 . \end{aligned} \tag{37}$$

In other words, each entry of $\varphi_{i,k}$ can be characterized as the sum of three harmonics and a constant offset that is large with respect to the amplitude of the three harmonic components. Since the cost function $\varphi_k = \sum_{i=1}^{N} \varphi_{i,k}$ and the determinant of φ_k involve further products and sums of its elements, coupling between the different UAV headings will be introduced. However, due to the relationship in (37), the coupling is relatively small compared to the effect of the constant offset term and the sum of first-order sinusoidal terms, where the first order terms are dependent on only one UAV heading $\psi_{i,k}$. This observation leads to the idea of decoupling the N-dimensional optimization problem into N one-dimensional optimization problems. The cost function $|\varphi_k|$ will produce sinusoidal harmonics up to the 12th order, but due to the observation in (37), only harmonics up to the 2nd order are required for sufficient accuracy. Thus, the criterion can be written in the following general form:

$$J(\psi_{i,k}) = \alpha_{i,1}^k \sin(\psi_{i,k} + \theta_{i,1}^k) + \alpha_{i,2}^k \sin(2\psi_{i,k} + \theta_{i,2}^k) + \beta_{i,k} \ + n(i,k), \tag{38}$$

where $\alpha_{i,m}^k, \theta_{i,m}^k, \beta_{i,k}, m = 1, 2$ are unknown and independent of $\psi_{i,k}$, and only $\beta_{i,k}$ depends on the headings of the other UAVs. Any errors in this approximation are absorbed into $n(i,k)$.

The approximation in (38) holds under the assumptions in (36). In situations where the range of the target to the UAVs is much larger than the UAVs' velocity and the estimated target velocity, this approximation will work well, as can be seen from the simulations in Section IV-B. As the target gets close to the UAVs, higher order effects become important and the UAV headings become increasingly coupled; in such scenarios the optimal heading should be found using a search of the cost function in (*i.e.*, (18)).

REFERENCES

[1] J. Ousingsawat and M. Campbell, "Establishing trajectories for multi-vehicle reconnaissance," in *Proceedings of the AIAA Guidance, Navigation, and Control Conference*, Aug. 2004, pp. 2188–2199.

[2] ——, "Optimal cooperative reconnaissance using multiple vehicles," *AIAA Journal of Guidance, Control, and Dynamics*, vol. 30, no. 1, pp. 122–132, 2007.

[3] M. Hernandez, T. Kirubarajan, Y. Bar-Shalom, Q. Ltd, and U. Malvern, "Multisensor resource deployment using posterior Cramer-Rao bounds," *Aerospace and Electronic Systems, IEEE Transactions on*, vol. 40, no. 2, pp. 399–416, 2004.

[4] A. Sinha, T. Kirubarajan, and Y. Bar-Shalom, "Autonomous ground target tracking by multiple cooperative uavs," in *IEEE Aerospace Conference*, 2005, pp. 1–9.

[5] M. Kovacina, D. Palmer, G. Yang, and R. Vaidyanathan, "Multi-agent control algorithms for chemical cloud detection and mapping using unmanned air vehicles," in *IEEE/RSJ Int. Conf. on Intelligent Robots and System.*, vol. 3, 30 Sept.-5 Oct. 2002, pp. 2782–2788vol.3.

[6] D. R. Keller, T. K. Moon, and J. H. Gunther, "Narrowband source localization from a moving array of sensors," in *Proc. 40th Asilomar Conf. Signals, Systems, and Computers*, 2006, pp. 2285–2289.

[7] G. J. Toussaint, P. De Lima, and D. J. Pack, "Localizing RF Targets with Cooperative Unmanned Aerial Vehicles," in *Proceedings of the American Control Conference*, 9-13 July 2007, pp. 5928–5933.

[8] D. Pack, G. York, and R. Fierro, "Information-based cooperative control for multiple unmanned aerial vehicles," in *Proc. IEEE Int. Conf. on Networking, Sensing and Control.*, 2006, pp. 446–450.

[9] K. Zhou and S. Roumeliotis, "Optimal Motion Strategies for Range-Only Distributed Target Tracking," *Proceedings of the American Control Conference*, pp. 5195–5200, 2006.

[10] S. Martinez and F. Bullo, "Optimal sensor placement and motion coordination for target tracking," *Automatica*, vol. 42, no. 4, pp. 661–668, 2006.

[11] M. L. Hernandez, "Optimal sensor trajectories in bearings-only tracking," in *Proceedings of the Seventh International Conference on Information Fusion*, P. Svensson and J. Schubert, Eds., vol. II. Mountain View, CA: International Society of Information Fusion, Jun 2004, pp. 893–900.

[12] Y. Oshman and P. Davidson, "Optimization of observer trajectories for bearings-only target localization," *IEEE Trans. Aerosp. Electron. Syst.*, vol. 35, no. 3, pp. 892–902, July 1999.

[13] B. Grocholsky, A. Makarenko, and H. Durrant-Whyte, "Information-theoretic coordinated control of multiple sensor platforms," in *Proc. IEEE Int. Conf. Robotics and Automation*, vol. 1, 2003, pp. 1521–1526.

[14] S. Maheswararajah and S. Halgamuge, "Mobile sensor management for target tracking," in *2nd International Symposium on Wireless Pervasive Computing*, 2007, pp. 506–510.

[15] A. Baras, J.S.; Bensoussan, "Sensor scheduling problems," in *Proceedings of the IEEE Conference on Decision and Control*, vol. 3, December 1988, pp. 2342–2345.

[16] V. Gupta, T. Chung, B. Hassibi, and R. Murray, "On a stochastic sensor selection algorithm with applications in sensor scheduling and sensor coverage," *Automatica*, vol. 42, no. 2, pp. 251–260, 2006.

[17] Y. He and K. Chong, "Sensor scheduling for target tracking in sensor networks," in *Proceedings of the IEEE Conference on Decision and Control*, December 2004, pp. 743–748.

[18] L. Kaplan, "Global node selection for localization in a distributed sensor network," *IEEE Trans. Aerosp. Electron. Syst.*, vol. 42, no. 1, pp. 113–135, Jan. 2006.

[19] ——, "Local node selection for localization in a distributed sensor network," *IEEE Trans. Aerosp. Electron. Syst.*, vol. 42, no. 1, pp. 136–146, Jan. 2006.

[20] K. Mehrotra, C. Mohan, R. Niu, and P. Varshney, "Temporally staggered sensors in multi-sensor target tracking systems," *IEEE Trans. Aerosp. Electron. Syst.*, vol. 41, no. 3, pp. 794–808, July 2005.

[21] M. Moges and T. Robertazzi, "Wireless sensor networks: scheduling for measurement and data reporting," *IEEE Trans. Aerosp. Electron. Syst.*, vol. 42, no. 1, pp. 327–340, Jan. 2006.

[22] O. Erdinc, P. Willett, and S. Coraluppi, "Multistatic sensor placement: A tracking approach," in *Information Fusion. 9th International Conference on*, July 2006, pp. 1–8.

[23] K. Punithakumar, T. Kirubarajan, and M. Hernandez, "Multisensor deployment using pcrlbs, incorporating sensor deployment and motion uncertainties," *IEEE Trans. Aerosp. Electron. Syst.*, vol. 42, no. 4, pp. 1474–1485, October 2006.

[24] D. Keller, T. Moon, and J. Gunther, "Source localization from moving arrays of sensors," in *Proc. 39th Asilomar Conf. Signals, Systems, and Computers*, 2005, pp. 452–456.

[25] G. Gu, P. Chandler, C. Schumacher, A. Sparks, and M. Prachter, "Optimal cooperative sensing using a team of uavs," *IEEE Trans. Aerosp. Electron. Syst.*, vol. 42, no. 4, pp. 1446–1458, 2006.

[26] R. Beard, D. Kingston, M. Quigley, D. Snyder, R. Christiansen, W. Johnson, T. McLain, and M. Goodrich, "Autonomous Vehicle Technologies for Small Fixed-Wing UAVs," *Journal of Aerospace Computing, Information, and Communication*, vol. 2, no. 1, pp. 92–108, 2005.

[27] N. J. Willis, *Bistatic Radar*. Artech House, Boston, 1991.

[28] H. Van Trees, *Radar-Sonar Signal Processing and Gaussian Signals in Noise*. John Wiley & Sons Inc, 2001.

[29] H. Griffiths, "From a different perspective: principles, practice and potential of bistatic radar," *Radar Conference. Proceedings of the International*, pp. 1–7, 2003.

[30] M. I. Skolnik, *Radar Handbook*. McGraw-Hill, 1990.

[31] M. Jackson, "The geometry of bistatic radar systems," *IEE Proceedings, Part F-Communications, Radar*, vol. 133, no. 7 pt F, pp. 604–612, 1986.

[32] T. Tsao, M. Slamani, P. Varshney, D. Weiner, H. Schwarzlander, and S. Borek, "Ambiguity function for a bistatic radar," *IEEE Trans. Aerosp. Electron. Syst.*, vol. 33, no. 3, pp. 1041–1051, 1997.

[33] N. J. Willis and H. D. Griffiths, Eds., *Advances in Bistatic Radar*. Scitech Publishing, Inc., 2007.

[34] P. Zhan, D. Casbeer, and A. L. Swindlehurst, "A Centralized Control Algorithm for Target Tracking with UAVs," *The Thirty-Ninth Asilomar Conference on Signals, Systems and Computers*, pp. 1148–1152, Oct. 2005.

[35] D. Casbeer, P. Zhan, and A. L. Swindlehurst, "A Non-search Optimal Control Solution for a Team of MUAVs in a Reconnaissance Mission," *Proc. of the IEEE Int. Conf. on Acoustic, Speech and Signal Processing*, pp. 1169–1172, 2006.

[36] P. Peebles, *Radar Principles*. A Wiley-Interscience Publication, 1998.

[37] T. Abatzoglou and G. Gheen, "Range, radial velocity, and acceleration MLE using radar LFM pulse train," *IEEE Trans. Aerosp. Electron. Syst.*, vol. 34, no. 4, pp. 1070–1083, 1998.